JOURNAL OF PROPULSION AND POWER
Vol. 12, No. 6, November–December 1996

Exit-Plane Electrostatic Probe Measurements of a Low-Power Arcjet

Rodney L. Burton* and Scott A. Bufton†
University of Illinois at Urbana–Champaign, Urbana, Illinois 61801

Improved understanding of the flow processes in a 1-kW hydrazine constricted arcjet is achieved with multiple electrostatic probe surveys in the exit-plane region of the plume. Quadruple, triple, and single electrostatic probe techniques are utilized for measurements of the electron temperature T_e, density n_e, and ratio of ion axial velocity to most probable thermal speed $u_i/c_{m,H^+}$. Centerline axial profiles of T_e and n_e are presented for 2.2–6.2 mm downstream of the exit-plane, yielding T_e = 6600 K ± 15% and n_e = 3.6 × 10^{12} cm^{-3} ± 60% close to the thruster exit. Quadruple probe theory is modified to account for radial gradients in T_e and n_e over the probe radial dimension, and is used to extract exit-plane radial T_e and n_e profiles. Floating probe measurements yield estimates of the radial electric-field profile at the thruster exit, implying a small amount of current and ohmic heating downstream of the exit-plane.

Nomenclature

A_k = electrode geometric surface area of electrode k, m^2
c_m = most probable thermal speed, m/s
E = electric field, V/m
e = electron charge, C
f = ion composition parameter, n_{H^+}/n_e
I = current, A
I_b = Bohm sheath ion current, A
I_t = current to electrode tip, A
j = current density, A/m^2
k = Boltzmann constant, J/K
L = electrode length, mm
m = particle mass, kg
n = particle density, cm^{-3}; summation integer
P_k = designation for electrode k
Q = collision cross section
r = radius, mm
s = electrode spacing, mm
T = temperature, K, eV
u_i = ion flow velocity, m/s
V_d = electrode relative bias voltage, V
V_f = floating probe voltage, V
V_p = plasma potential, V
V_s = sheath potential, V
x = axial distance from thruster exit, mm
x_{H^+,N^+} = wake effect collection area parameters
α = degree of ionization
Γ = mathematical gamma function
δ = flow divergence angle, deg
ε_d = dissociation energy, eV
κ = correction to n_e caused by N^+ ions
λ_D = Debye length, mm
λ_{mfp} = mean free path, mm
μ = equal to $(m_{H^+}/m_{N^+})^{1/2}$
σ = electrical conductivity, mho/m; standard deviation, mm
τ_L = electrode end effect parameter
ϕ = e/kT_e, V^{-1}

Subscripts
e, i, n = electron, ion, neutral species
g = gas
r = radial
m = measured quantity
1–4 = electrode designation

Received Nov. 2, 1994; revision received Nov. 30, 1995; accepted for publication Aug. 17, 1996.

*Associate Professor, Department of Aeronautical and Astronautical Engineering. Associate Fellow AIAA.

†Ph.D. Candidate, Department of Mechanical and Industrial Engineering. Student Member AIAA.

Introduction

ELECTROSTATIC probes have found much use in experimentally determining plasma parameters in space and laboratory plasmas, both to investigate arcjet efficiency and to validate numerical models.[1–6] Several authors[7–11] have employed classical Langmuir[12] single probes in the characterization of low-power arcjet plumes. While single probes are appealing because of their relatively simple construction, interpreting the probe voltage–current (V–I) characteristic is unwieldy. A viable alternative is the triple electrostatic probe,[13] which allows simultaneous measurement of T_e and n_e without the necessity of a voltage sweep and generation of a corresponding probe V–I characteristic. The utility of triple probes for electric propulsion devices has been demonstrated in magnetoplasmadynamic (MPD) thruster plumes[14–17] and in a 1-kW hydrogen arcjet plume.[18] Additionally, a general review of electrostatic probe techniques and their uses in electric propulsion devices has recently been presented.[19]

Under certain conditions, the crossed-probe technique[20–23] can be used to measure u_i/c_m (=plasma velocity/ion most probable thermal speed) in flowing plasmas. The quadruple electrostatic probe[24–28] combines the crossed-probe and triple-probe techniques for simultaneous measurements of T_e, n_e, and u_i/c_m. The utility of the quadruple probe has been demonstrated in an MPD thruster,[24,25] and more recently, in the very near-field plume of a 1-kW hydrazine arcjet.[26–28]

Despite the utility of triple- and quadruple-probe techniques, interpretation of the probe response can be difficult in regions of the plume where variations in plasma parameters are large over the finite dimensions of the probe. In particular, axial gradients (along the electrode length) and radial gradients (perpendicular to the electrodes) must be considered when interpreting measurements (T_e, n_e) made with multiple electrode probes. Conventional triple- and quadruple-probe analyses assume no plasma gradients over the probe volume, which is strictly true only in a uniform plasma or on the axis of an azimuthally symmetric beam plasma. This article demonstrates the effect of axial and radial gradients on the quadruple-probe response in the arcjet near-field plume, presents a modified quadruple-probe analysis that is capable of handling radial gra-

dients in T_e and n_e over the probe width, and provides experimental results using the revised theory.

Quadruple-Probe Technique

Figure 1 shows an electrical schematic diagram of the quadruple probe, consisting of three cylindrical electrodes (P_1, P_2, and P_3), which are aligned with the plasma flow vector and one electrode (P_4), which is perpendicular to the plasma flow. P_3 and P_4 are biased at constant voltages V_{d3} and V_{d4} relative to P_1, and P_2 assumes the floating potential V_f of the local plasma ($I_2 = 0$). The circuit including electrodes 1, 3, and 4 is electrically floating such that ion current collected at P_3 and P_4 is balanced by the electron current collected at P_1, thereby determining the potential difference between electrodes 1 and 2 $V_{d2}(T_e)$. The three aligned electrodes 1–3 comprise the triple probe and yield simultaneous measurements of n_e and T_e. The addition of the perpendicular electrode P_4 allows the measurement of the parameter u_i/c_m, determined from the ratio I_4/I_3 for crossed electrostatic electrodes with $V_{d3} = V_{d4}$. For the quadruple probe, the measured quantities are the electrode currents I_3 and I_4 and V_{d2}. Currents I_3 and I_4 are determined by measuring voltage drops across resistors ($R_3 = R_4 = 100\ \Omega$). The electrode bias voltages V_{d3} and V_{d4} are provided by 12V batteries, such that $V_{d3} = V_{d4}$. The theoretical probe response, as given in Eq. (1), is insensitive to the bias voltage over the range $8 < V_{d3} < 16$ V.

Probe Geometry

A schematic diagram of the quadruple probe used in this study is shown in Fig. 2. The probe is comprised of four individual tungsten wire electrodes of 0.25 mm diameter with an exposed length of 2.5 mm for electrodes 1–3 and 2.0 mm for the perpendicular electrode 4. The location of the perpendicular electrode has been modified from that of previous probes, to coincide with the axial midpoint of the three aligned electrodes. Each wire is mounted in round single-bore alumina (Al_2O_3) tubing, which is in turn mounted in, and supported by, thin-wall stainless-steel tubing. This assembly is mounted in a larger stainless-steel tube to facilitate connecting the probe tip to the probe-positioning mechanism discussed later. Inside this larger tubing is a four-bore alumina tube that electrically insulates the four probe leads. A high-temperature ceramic-based adhesive[29] is used to bond each of the probe electrodes and components in place. A small quantity of adhesive is placed at the junction between P_4 and its single-bore alumina tube to electrically insulate part of the electrode, thereby reducing the error associated with determining the geometric surface area A_4 (Fig. 2).

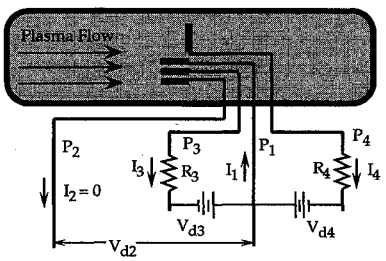

Fig. 1 Quadruple-probe electrical schematic diagram.

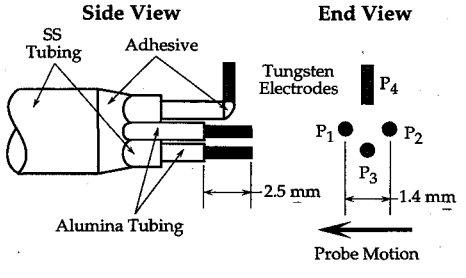

Fig. 2 Schematic of quadruple-probe tip swept through the arcjet plume.

The center-to-center separation between electrodes 1 and 2 is 1.4 mm. This spacing, along with electrode lengths of 2.5 mm, allows an unaligned quadruple probe to tolerate flow divergence angles $\delta \sim 30$ deg, without shadowing of one electrode by the other. In an effort to minimize the effect of the probe geometry on the plasma flow, a stepped transition between an electrode and its support has been implemented. The diameter of the single-bore alumina electrode support is ~0.8 mm, which minimizes perturbations of the plasma flow at the support end. The exposed length of the single-bore alumina is ~5 mm. Ceramic adhesive is used to fill the void and ease the transition between the electrodes and the stainless-steel probe support tubing (Fig. 2).

Probe Length Scales

For the conditions expected at the exit-plane probe location ($T_e \sim 0.6$ eV, $n_e \sim 4 \times 10^{12}$ cm^{-3}), the Debye length is 3×10^{-4} cm and the ratio of electrode radius to Debye length $r_p/\lambda_D \sim 45$, so that the ion sheath surrounding the electrodes can be characterized as thin. For probe measurements 5 mm downstream, this ratio increases to $r_p/\lambda_D \sim 55$. The spacing s between electrodes 1 and 3 (Fig. 2) is ~1 mm, so that $s/\lambda_D > 250$ and the sheaths on adjacent electrodes do not interact.

To avoid strong sensitivity of the ion current to small misalignments between the flow vector and the electrode axis, the so-called end effect parameter[30] $\tau_L = (L/\lambda_D)(\sqrt{kT_e/m_i}/u_i)$ should be >50. For our plasma conditions, this parameter is conservatively estimated at $\tau_L > 250$. In addition, the electrodes ideally should be long enough that the Bohm sheath ion current collected along the cylinder length I_b is much larger than the current collected at the probe end caused by the convection of charged particles into the probe tip I_t. A first-order analysis of the ratio I_b/I_t for the conditions at the exit-plane shows $I_b/I_t > 30$, so that the error introduced to the collected ion current by neglecting the probe tip current is ~3%.

The radius r_p of the tungsten electrodes (Fig. 2) was chosen as a compromise between the thin sheath requirement ($r_p/\lambda_D >> 1$) and the condition of free molecular flow over the probe electrodes ($\lambda_{mfp}/r_p >> 1$). For the seven-species plasma expected at the exit-plane (H_2, N_2, H, N, H^+, N^+, and e), all relevant collision mean free paths were calculated. Other N–H molecular species, for example, NH and NH_3, exist in mole fractions less than $\sim 10^{-5}$ and are neglected.[31] The following assumptions are made in calculating mean free paths: $T_e = 7000$ K, $T_g = 2500$ K, $n_e = 4 \times 10^{12}$ cm^{-3}, and $n_{neutral} = 3 \times 10^{15}$ cm^{-3} with 10% dissociation at the thruster exit. The following mean free path ratios were calculated: $\lambda_{n-n}/r_p = 20$, $\lambda_{i-n}/r_p = 5$, $\lambda_{i-i}/r_p = 30$, $\lambda_{i-e}/r_p = 20$, $\lambda_{e-n}/r_p = 20$, and $\lambda_{e-e}/r_p = 30$. Clearly, the probe electrodes are operating in the collisionless regime. Additionally, $\lambda_{mfp}/\lambda_D > 200$ for all collisions, with an overwhelming majority of the collisions having $\lambda_{mfp}/\lambda_D > 1000$, indicating that the collisionless sheath assumption is appropriate.

Quadruple-Probe Response to a Uniform Plasma

Quadruple-probe analysis for a uniform plasma assumes the following:

1) The ion sheath surrounding the tungsten wires is thin compared to the wire radius ($r_p >> \lambda_D$).

2) Each probe electrode wire and sheath are collisionless ($\lambda_{mfp} >> r_p >> \lambda_D$).

3) The electron energy distribution is Maxwellian.

4) Velocity slip between plasma species is negligible.

5) Gradients over the probe geometry are negligible.

6) A wake region of low ion and electron density exists downstream of the perpendicular electrode P_4. The thin sheath assumption directly implies that the ion saturation current is independent of the electrode bias potential.

Derivation of quadruple probe response is similar to that for the triple probe and has been presented elsewhere.[24-28] In previous work[27,28] we presented some of the revisions necessary to allow the application of triple- and quadruple-probe theory to multicomponent (N_2–H_2) plasmas. In the present study, the probe is applied to a simulated hydrazine plume, with multiple species of ions present, whereas most of the previous applications of triple and quadruple probes have been for plasmas with one dominant species of positive ion. Single langmuir probes have been used in N_2–H_2 plasmas,[7-10] but their use is not contingent on knowledge of the species mole fractions.

In the present study, we present an important modification of the quadruple probe theory. Rather than utilizing an analytic expression for I_4, the current collected at electrode P_4, I_4 is related to the current collected at P_3 through the ratio of the measured quantities I_3 and I_4. The significance of this modification is that it completely removes errors in T_e and n_e measurements caused by assumptions regarding the effective current collection area of P_4. For a quadruple probe with electrode geometric surface areas $A_1 = A_2 = A_3$, and electrode biasing such that $V_{d3} = V_{d4}$, the following expression can be derived in a manner similar to that used in previous studies[24-28]:

$$1 = \frac{1 + \exp(\phi V_{d3}) - 2\exp[\phi(V_{d3} - V_{d2})]}{(I_4/I_3)\{\exp[\phi(V_{d3} - V_{d2})] - 1\}} \tag{1}$$

Since V_{d3} is prescribed and V_{d2} and (I_4/I_3) are determined experimentally, Eq. (1) determines $T_e = e/k\phi$ through iteration.

The ion saturation current density j_i is related to measured quantities by

$$j_i = \frac{(I_3/A_3)(1 + I_4/I_3)}{\exp(\phi V_{d2}) - 1} \tag{2}$$

Normally, Eq. (2) is used to determine n_e from I_3 and V_{d2} by relating j_i to the electron density through a Bohm sheath analysis. For a plasma with only one species of positive ion, the Bohm analysis gives[13]

$$j_i = en_e(kT_e/m_i)^{1/2}\exp(-\tfrac{1}{2}) \tag{3}$$

For a plasma with multiple ion species, Eq. (3) must be modified. Assuming that each collected positive ion is accelerated through the Bohm sheath in a collisionless manner and collected by the probe, j_i becomes

$$j_i = e(kT_e)^{1/2}\exp\left(-\frac{1}{2}\right)\left\{\sum_{j=1}^{\text{no. species}}\left[\frac{n_j}{(m_j)^{1/2}}\right]\right\} \tag{4}$$

Assuming equilibrium dissociation of $2H_2 + N_2$ in the arcjet constrictor with each species concentration frozen downstream of the constrictor to the exit-plane, numerical equilibrium codes predict H^+ and N^+ as the dominant positive ions present at measurable levels.[31] The Bohm ion saturation current is then

$$j_i = e(kT_e)^{1/2}\exp\left(-\frac{1}{2}\right)\left[\frac{n_{H^+}}{(m_{H^+})^{1/2}} + \frac{n_{N^+}}{(m_{N^+})^{1/2}}\right] \tag{5}$$

For $n_e = n_{H^+} + n_{N^+}$, Eqs. (2) and (5) yield

$$n_e = \frac{\kappa(I_3/A_3)[1 + (I_4/I_3)]\exp(\frac{1}{2})(m_{H^+})^{1/2}}{e(kT_e)^{1/2}[\exp(\phi V_{d2}) - 1]} \tag{6}$$

In Eq. (6), κ represents the effect of multiple-ion species on the probe response to electron density:

$$\kappa = \frac{1 + (n_{N^+}/n_{H^+})}{1 + \mu(n_{N^+}/n_{H^+})} \tag{7}$$

where $\mu = (m_{H^+}/m_{N^+})^{1/2}$. For a plume containing only H^+, $n_{N^+} = 0.0$ and κ reduces to unity, such that Eq. (6) reduces to single component (H^+) form.

Experimental observations[32,33] show that low nitrogen ion densities are found near the exit-plane in ammonia and hydrazine arcjets. It is suggested that this is consistent with a plasma dominated by charge exchange collisions in the expanding nitrogen–hydrogen propellant, and with the preferential dissociation of H_2 ($\varepsilon_d = 4.48$ eV) over N_2 ($\varepsilon_d = 9.61$ eV). The arcjet exit-plane plasma is highly dissociated and partially ionized, with $T_e > T_g$, and the estimated range of gas temperature is $T_g < 6000$ K. Dissociation and ionization by electron collisions are negligible, because of low electron density and temperature, and atomic nitrogen rapidly undergoes charge-exchange collisions with hydrogen, the cross section for which is on the same order of magnitude as N–H momentum transfer collisions. Neglecting radial species diffusion and convective effects, charge exchange gives $H + N^+ \leftrightarrow H^+ + N$, and the two charge exchange reactions balance in steady state. Writing these volumetric collision rates in the form nQv, with relative thermal speeds $v_{H,N} \approx v_H$, and cross sections $Q_{H-N^+} \approx Q_{N-H^+}$ gives

$$n_{N^+}/n_{H^+} = n_N/n_H \tag{8}$$

which directly implies a low nitrogen ion density in the exit-plane. This result is supported by equilibrium calculations for $T < 7500$ K at 1 atm.[31] Thus, the relative nitrogen ion density is effectively determined by dissociation through T_g and not I_e. For $T_g < 6000$ K, $n_{N^+}/n_{H^+} < 0.1$ and $\kappa < 1.07$, indicating a ~7% increase in n_e caused by the presence of nitrogen ion probe current.

Ion Speed Ratio Measurements

The use of crossed electrostatic probes for measuring the ion speed ratio and the implementation of the crossed probe technique into the quadruple probe have been presented elsewhere.[20-28] For a cylindrical electrode oriented at an angle θ relative to the plasma flow, the collected ion current is a function of the quantity $(u_i/c_m)\sin\theta$, where $c_m = (2kT_i/m_i)^{1/2}$. For the case of two equally biased electrodes, with one probe aligned with the flow vector and the other one normal to it, the single-species collected ion current ratio for the thin sheath case is[22]

$$\frac{I_4}{I_3} = \frac{2A_4}{\sqrt{\pi}A_3}\exp\left[-\left(\frac{u_i}{c_m}\right)^2\right]\sum_{n=0}^{\infty}\left[\frac{\left(\frac{u_i}{c_m}\right)^n}{n!}\right]^2\Gamma\left(n + \frac{3}{2}\right) \tag{9}$$

To apply the crossed-probe technique to the multicomponent (H_2–N_2) plasmas of interest here, significant revisions must be made to Eq. (9). Previously, a single-component form of the Maxwellian velocity distribution was assumed for the electrode ion collection expression.[20] For the present study, this expression has been rederived using a two-component form of the Maxwellian velocity distribution. The derivation is similar to the single-component case, and results in a contribution to the ratio I_4/I_3 from each of the collected ion species. For the two species of ions assumed present, the ion composition is defined by $n_{H^+}/n_e = f$ and $n_{N^+}/n_e = (1 - f)$. The resulting expression for the measured current ratio is

$$\frac{I_4}{I_3} = C\left\{f(x_{H^+})\exp\left[-\left(\frac{u_i}{c_{m,H^+}}\right)^2\right]\sum_{n=0}^{\infty}\left[\frac{\left(\frac{u_i}{c_{m,H^+}}\right)^n}{n!}\right]^2 \times \Gamma\left(n + \frac{3}{2}\right) + \mu(x_{N^+})(1 - f)\exp\left[-\left(\frac{u_i}{\mu c_{m,H^+}}\right)^2\right] \times \sum_{n=0}^{\infty}\left[\frac{\left(\frac{u_i}{\mu c_{m,H^+}}\right)^n}{n!}\right]^2\Gamma\left(n + \frac{3}{2}\right)\right\} \tag{10}$$

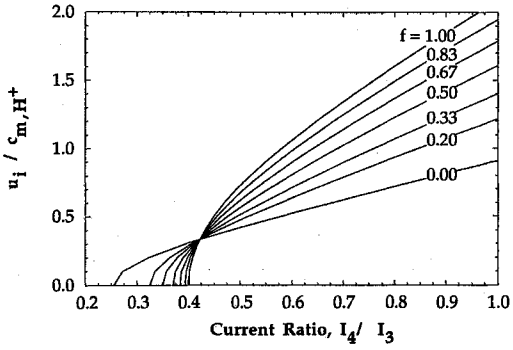

Fig. 3 Velocity ratio $u_i/c_{m,H^+}$ vs I_4/I_3 for 0.0 < f < 1.0, where $f = n_{H^+}/n_e$. For this study, $f \sim 0.9$, corresponding to $\kappa = 1.07$.

where the constant C is given by

$$C = \frac{2A_4}{\sqrt{\pi}A_3[f + (1 - f)\mu]} \tag{11}$$

In Eq. (10), the first term in the braces { } is the H^+ contribution, and the second term is the N^+ contribution, where $c_{m,N^+} = \mu c_{m,H^+}$ has been introduced. Note that each of the terms is weighted by the relative density of its corresponding ion [f, $(1 - f)$].

Because a wake is formed behind P_4, only a portion (x_{H^+}, x_{N^+}) of the electrode area A_4 collects ions. Because the extent of the wake effect is determined by the relative magnitudes of the directed ion velocity u_i and thermal speed of the ions, x_{H^+} and x_{N^+} are not necessarily equal. For $T_g = T_i = 2500$ K and a directed velocity $u_i \sim 6500$ m/s, $u_i/c_{m,H^+} \sim 1$ and $u_i/c_{m,N^+} \sim 4$.

Several references discuss the wake effect for high-speed flows.[21-24] It has been postulated and experimentally verified for an argon plasma at $u_i/c_m \sim 1$, that the wake effect causes the effective collection area to be half of the geometric electrode area.[22] Since $u_i/c_{m,H^+}$ is expected to be ~ 1, x_{H^+} is assumed to be $\frac{1}{2}$, so that only the front half of P_4 collects ions. For the nitrogen ions, the wake effect reduction in collection area is more pronounced. Since the directed velocity u_i is several times c_{m,N^+}, N^+ is collected by the projected area[24,25] of P_4, such that $x_{N^+} = 1/\pi$.

Given an estimate of the plasma composition f, Eq. (10) becomes an expression for $u_i/c_{m,H^+}$ vs the measured current ratio I_4/I_3. Equation (10) is plotted in Fig. 3 for $0 \leq f \leq 1$, $x_{H^+} = 1/2$ and $x_{N^+} = 1/\pi$. Pure H^+ collection is represented by $f = 1.0$, $2H^+ + N^+$ collection by $f = 0.67$, and pure N^+ collection by $f = 0.0$.

We note that, given an independent measure of the directed plasma velocity u_i, Fig. 3 can be used to determine c_{m,H^+} [$=(2kT_i/m_{H^+})^{1/2}$] and, hence, estimate the gas temperature $T_g = T_i$.

Quadruple-Probe Response to Plasma Gradients

The quadruple-probe response is expected to be influenced by radial plasma gradients over the probe width and by axial plasma gradients along the probe length. The nature of the experimental apparatus did not permit probe sweeps in the axial direction. The results of successive radial probe sweeps at different axial locations given later indicate a small axial n_e gradient, which the axial probe electrodes average over their length.

As a foundation for fully understanding the quadruple probe response to plasma gradients, an initial investigation of the physical symmetry of the near-field arcjet plume was performed. A classical single langmuir probe (P_3 in Fig. 2) was used to measure the current collected during several radial sweeps across the thruster exit-plane. During these sweeps, the electrode tip was located 1.0 mm from the thruster exit and biased from −8.0 (ion collection) to 6.0 V (electron collection), relative to facility ground. The smoothed single-probe surveys, demonstrating the symmetric nature of the arcjet near-field plume, are summarized in Fig. 4. For a given radius, these data constitute a langmuir probe V–I characteristic. At $r = 0.0$ mm, this V–I characteristic yields $T_e \sim 0.6$ eV. The uncertainty in T_e is ±15%, created by uncertainties in theory and data reduction, and to a lesser extent by uncertainties in measured quantities.

The results of a typical quadruple-probe radial sweep are shown in Fig. 5. Like the single-probe data presented earlier (Fig. 4), quadruple-probe measurements at the thruster exit-plane reveal a symmetric profile for the measured electrode current I_3. However, the measured potential difference V_{d2} is not symmetric with radius as a result of the steep radial gradient in n_e off-axis and, to a lesser extent, the radial gradient in T_e. These gradients, which are perpendicular to the quadruple-probe electrodes and the arcjet thrust axis, cause the local values of T_e and n_e to differ from electrode P_1 to electrode P_2.

In the presence of radial plasma gradients, the individual electrode current equations[25,26] must be written in terms of the plasma parameters (T_e, n_e) at each electrode. Noting that $\phi V_{d3} >> 1$, these equations can be solved explicitly for V_{d2} and I_3 in terms of the radial profiles of T_e and n_e:

$$V_2 = V_2(T_{e2}, \kappa) \tag{12}$$

$$V_1 = V_1(T_{e1}, T_{e3}, n_{e1}, n_{e3}, I_4/I_3, \kappa) \tag{13}$$

$$V_{d2} = V_2 - V_1 \tag{14}$$

$$I_3 = I_3(T_{e3}, n_{e3}, \kappa) \tag{15}$$

where the subscripts on the parameters T_e and n_e in Eqs. (12–15) denote the local value of those parameters at each of the electrodes (1–3) of the quadruple probe. The ratio I_4/I_3 is a

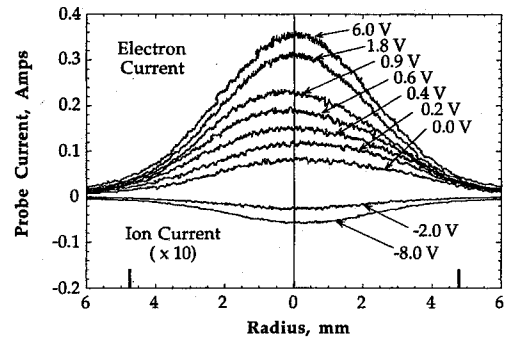

Fig. 4 Single-probe measurements demonstrating arcjet plume symmetry. Curve labels represent electrode bias voltages relative to ground. Cross plots at constant radii yield single-probe V–I characteristics.

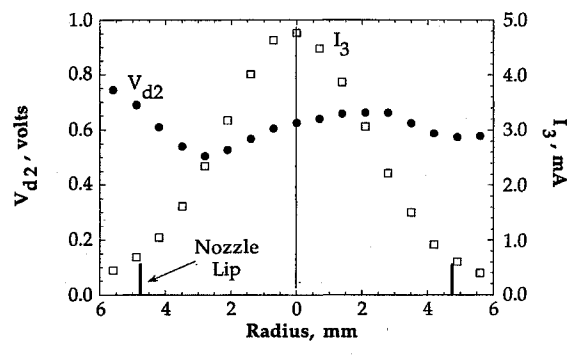

Fig. 5 Profiles of $I_3(r)$ and $V_{d2}(r)$ measured by the quadruple probe.

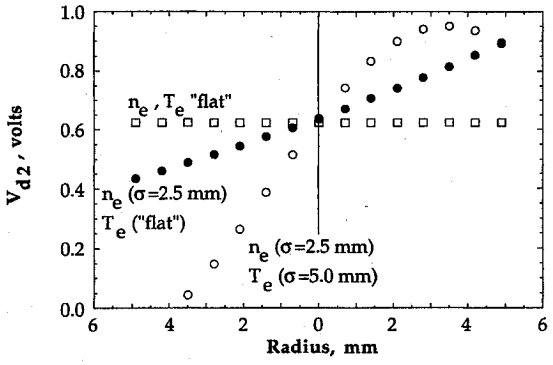

Fig. 6 Calculated quadruple-probe response to axisymmetric Gaussian profiles of T_e and n_e with standard deviation σ (mm). Probe wire separation = 1.4 mm (Fig. 2).

measured quantity, and κ is a function of the plasma composition discussed earlier. The current I_3 [Eq. (15)] displays no T_{e1} and n_{e1} dependence because electrode 3 collects ion saturation current, which is determined primarily by the local conditions at electrode 3. For axisymmetric plumes, the centerline experimental data are at zero-gradient conditions (Fig. 4) and can be used with Eqs. (1) and (6) to determine the centerline values of T_e and n_e.

Using the functional dependencies demonstrated in Eqs. (12–14), Fig. 6 displays the predicted quadruple-probe response V_{d2} vs radial position for the probe of Fig. 2, for both constant (standard deviation $\sigma = 1000$) and Gaussian ($\sigma = 2.5$ or 5) n_e and T_e profiles. For Gaussian n_e and constant T_e, V_{d2} increases monotonically across the thruster. For a Gaussian T_e distribution broader than n_e, the V_{d2} profile shows more asymmetry.

As an illustration for the case of constant T_e, Eqs. (12–14) can be solved analytically for V_{d2}, giving

$$V_{d2} = (kT_e/e)\ell n\{[1 + (I_4/I_3)](n_{e3}/n_{e1}) + 1\} \qquad (16)$$

In this equation the effect of the density gradient can be clearly seen. As the moving probe starts outside the plume and enters it, $n_{e3}/n_{e1} < 1$. At the axis $n_{e1} = n_{e3}$, and as the probe leaves the plume, $n_{e3}/n_{e1} > 1$. The result [Eq. (16)] is a monotonically increasing V_{d2} across the thruster face.

Given arbitrary profiles of $T_e(r)$ and $n_e(r)$, Eqs. (14) and (15) predict $V_{d2}(r)$ and $I_3(r)$. The inverse problem, of extracting n_e and T_e profiles from the measured V_{d2} and I_3, can also be solved. Since V_{d2} [Eq. (14)] is a strong function of T_e, and I_3 [Eq. (15)] is a strong function of n_e, there is sufficient uncoupling that an iterative routine can be used to find the unique $T_e(r)$ and $n_e(r)$ profiles that reproduce the measured V_{d2} and I_3 profiles. Starting with centerline values and assumed Gaussian profiles, the routine marches the probe position across the thruster face, while generating a new T_e profile. This updated profile is used with Eq. (15) to update $n_e(r)$, and the process is repeated until both profiles converge. Typically, five numerical iterations are required to reach convergence.

Gradients in Plasma Potential

Asymmetry in the measured V_{d2} signal is caused not only by radial gradients in T_e and n_e, but also by a radial gradient in V_p, since the individual electrode potentials (V_{1-4}) are defined relative to the plasma potential. A nonzero plasma potential gradient results in a different V_p at electrodes 1 and 2, which affects the V_{d2} measurement, but not that of I_3 and I_4, which draw saturation current. The potential difference V_{d2} is related to the measured potential difference $(V_2-V_1)_m$ through the local plasma potentials at electrodes 1 and 2 (V_{p1} and V_{p2}) by[27]

$$V_{d2} = (V_2 - V_1)_m - (V_{p2} - V_{p1}) \qquad (17)$$

so that the measured quantity $(V_2-V_1)_m$ must be corrected by $V_{p2}-V_{p1}$ to determine the electron temperature. Floating probe measurements discussed next show that this correction term is small within a few millimeters of the centerline.

Experimental Facilities

Electrostatic probe experiments were carried out at the exit-plane of a 1-kW arcjet thruster[34] operating at a flow rate of 50 mg/s of $2H_2 + N_2$ to simulate fully decomposed hydrazine propellant. The 2% thoriated tungsten nozzle is conical with a 20-deg half-angle, an exit diameter of 9.5 mm, and an area ratio of 225. Each component of the propellant was individually metered by unit instruments mass flow controllers and mixed in the propellant line. During steady-state operation, the thruster operated at 10.0 A and 112 V ($P/\dot{m}$ = 22.4 MJ/kg). Arc current was measured with a Hall effect current transducer. The thruster exhausted into a 1-m-diam × 1.5-m-long vacuum tank[26,27] at ~25 Pa during arcjet operation. Anode temperatures were monitored with an optical pyrometer, reaching ~1200 K during steady-state operation.

The electrostatic probes in the present study were accurately positioned and repeatably swept through the thruster plume with the probe mount system shown in Fig. 7. The complete assembly was fastened to a step motor (Fig. 7) mounted on a linear translation carriage.[26,27] The motor and probe assembly carriage is capable of ±5 cm linear translation perpendicular to the arcjet axis, allowing the probes to be manually swept through the plume at ~20 cm/s. Carriage and probe position were determined to 0.25 mm by a precision 10-kΩ linear potentiometer coupled to the carriage manual drive shaft, and calibrated against the outer diameter of the anode. The probe support arm is coupled directly to the motor shaft with the probe tip on the shaft axis, allowing probe angle to be varied (in 0.9-deg increments) without changing the probe tip location.

Probe elevation was repeatably located to within 0.5 mm by aligning the probe center with a line etched on the arcjet anode. The separation between the probe tips and the thruster exit-plane was reliably set to within 0.1 mm with a spark gap gauge. The arcjet mount deflection toward the probe is ~0.7 mm during evacuation of the vacuum tank. Any error associated with the arcjet exit-plane position because of this deflection is systematic and does not affect the relative spacing of subsequent axial measurement positions.

It has been shown[14] that probe contamination can have a marked effect on T_e measurements through drastic changes in the measured quantity V_{d2}. In the present study, the probe electrodes were cleaned thoroughly before each data acquisition session using ion bombardment cleaning[14] at 200 V below facility ground. Cleaning was performed in the arcjet plasma stream so that the electrodes would glow brightly during the process. Quadruple probe sweeps acquired before cleaning consistently yielded electron temperatures that were approximately double the postcleaning values. No electrode contam-

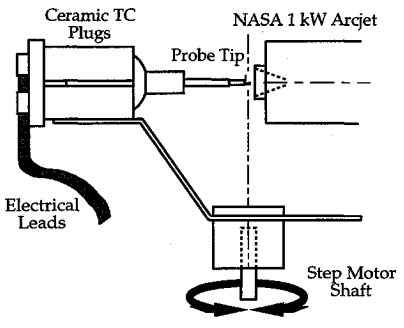

Fig. 7 Schematic diagram of quadruple-probe mount. The probe is translated horizontally perpendicular to the arcjet axis. The probe electrode axes are parallel to the thruster axis in this study.

ination effects were observed during each individual data acquisition session.

Experimental Results and Analysis

Experimental results are presented in an effort to quantify the extent of radial and axial gradients in T_e and n_e and their effect on quadruple-probe response. Based on previous quadruple-probe measurements,[27] the arcjet reaches steady-state operation after approximately 6 min, a result consistent with previously reported data.[34] All of the data presented in this article were acquired after ~10 min of continuous arcjet operation. Additionally, current ripple (±10%) inherent in the arcjet power processing unit has a marked influence on electrostatic probe plume measurements.[18,26,28] Here, the measured ripple in the probe raw data has been smoothed and mean values of T_e, n_e, and $u_i/c_{m,H^+}$ are presented.

Axial T_e and n_e Profiles

From previous measurements, it is evident that significant axial gradients of n_e exist on axis, inside the nozzle near the thruster exit-plane.[9,35,36] If these gradients are also large at the quadruple-probe measurement position, the probe theory must be modified accordingly. To quantify the extent of axial gradients in T_e and n_e over the 2.5-mm quadruple-probe electrode length, centerline data were acquired for five probe tip locations from 1 to 5 mm from the thruster exit, yielding the axial centerline profiles of T_e and n_e shown in Fig. 8. As a check to ensure that the presence of the perpendicular electrode (P_4) does not influence the T_e and n_e data, independent measurements were made with a triple probe at the x = 2.2-mm axial location.

The quadruple- and triple-probe T_e and n_e data were consistent within 5%, well within the experimental error associated with the experiment. This is not a surprising result, since in the limit $I_4/I_3 \rightarrow 0$, Eqs. (1) and (6) reduce to the triple-probe equations for T_e and n_e. Recall that single langmuir probe surveys also verify the multiple-probe T_e measurements, as described earlier.

Uncertainty in the quadruple- and triple-probe T_e values is estimated as ±15%, because of uncertainty in the V_{d2} measurement, and to assumptions in the quadruple- and triple-probe analyses. A ±17% uncertainty in the ratio I_4/I_3 only results in a ±4% sensitivity in T_e in Eq. (1). Experimental uncertainty in n_e results from the determination of electrode surface area, the current I_3, uncertainty in T_e, and fundamental assumptions in the quadruple- and triple-probe theories. Because of these assumptions (e.g., the Bohm sheath model for current collection), the uncertainty in n_e measurements is ±60%.[14]

The electron temperature (Fig. 8) varies from 6700 to 3600 K (~0.6–0.3 eV) between $2.2 < x < 6.2$ mm from the thruster exit. These results are consistent with previous far-field plume results of $T_e \sim 0.2$–0.3 eV for $30 < x < 150$ mm and $T_e \sim 0.1$–0.2 eV for x = 320 mm.[8,9] Further, the present data seem to corroborate previous estimates of $T_e \geq 0.5$ eV near the arcjet exit, based on arguments that T_e is on the order of the atomic excitation temperature.[36]

Results for the electron density axial profile are also shown in Fig. 8. Over the range of probe locations investigated, n_e drops by only ~30%, with dn_e/dx slightly higher near the thruster exit. A similar trend has been noted for hydrogen atom density measurements in a 1-kW hydrogen arcjet.[37] In that study, a decrease in centerline H atom density of 40% was observed between 2–6 mm from the thruster exit-plane. The n_e gradient based on the present data ($dn_e/dx \sim -0.5 \times 10^{12}$ cm^{-3}/mm at x = 2–3 mm) is small compared with the axial gradient indicated in the nozzle interior and at the exit-plane. Thus, large axial variations in the n_e gradient (large d^2n_e/dx^2) are likely to be present in the thruster near-field plume, $x <$ 2 mm.

From Fig. 8, it is apparent that the quadruple-probe results represent plasma conditions averaged over the axial dimension (2.5 mm) of the probe axial electrodes. The axial gradient in n_e is sufficiently small over the electrode length so that its effect on the quadruple-probe response is minor, and a corresponding correction to the probe response is deemed unnecessary. However, the large n_e gradients presumed to exist at the thruster exit-plane ($-2 < x < 2$ mm) require extra care in locating and reporting probe positions for both optical and intrusive measurement techniques.

Radial T_e and n_e Profiles

Data for V_{d2} and I_3 are shown for a radial sweep at x = 2.2 mm in Fig. 5. These data and the modified quadruple-probe theory [Eqs. (12–15)] are used to solve for the radial profiles $T_e(r)$ and $n_e(r)$. This analysis indicates that the T_e profile is very flat near the centerline ($r < 3$ mm) and nearly uniform at $T_e \sim 0.6$ eV. This uniform T_e is used to determine the radial n_e profile as shown in Fig. 9.

Far from the centerline, uncertainty in n_e increases because of misalignment between electrode 3 and δ. A recent study has shown that T_e measurements can also be artificially increased by electrode misalignment with the flow vector.[16] It was demonstrated that T_e measurements in the plume of an MPD thruster by means of a triple probe yielded T_e values for a 30-deg misalignment that were ~6% higher than measurements made with an aligned probe. Results presented in this study are limited to regions of the plume on or near the centerline, where the misalignment is small, so that variations caused by this effect are a few percent.

Ion Speed Ratio

The measured currents I_3 and I_4 and the current ratio I_4/I_3 are plotted in Fig. 10 for x = 2.2 mm. The measured current ratio of $I_4/I_3 = 0.60$, along with $\kappa = 1.07$ ($f \sim 0.9$), yields $u_i/c_{m,H^+} = 1.0 \pm 15\%$ [see Eq. (10)]. The value of $u_i/c_{m,H^+}$ is highly dependent on the plasma composition parameter f (Fig.

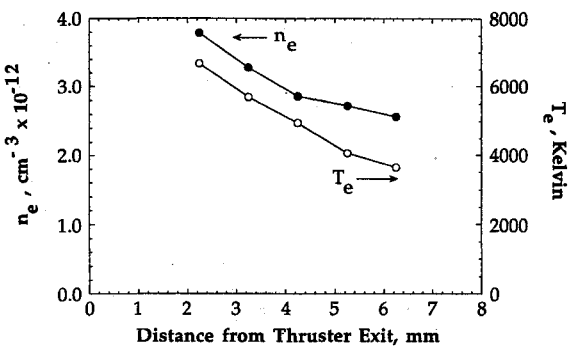

Fig. 8 Axial variation of T_e and n_e. The n_e gradient is $\sim -0.5 \times 10^{12}$ cm^{-3}/mm at x = 2.2 mm. Experimental uncertainties in T_e and n_e are ±15 and ±60%, respectively.

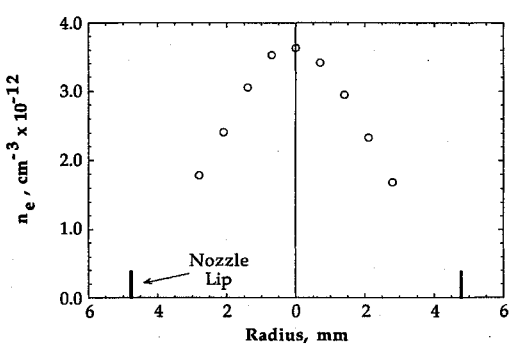

Fig. 9 Measured n_e radial profile for the quadruple probe centered at x = 2.2 mm from the thruster exit-plane. Experimental uncertainty in n_e is ±60%.

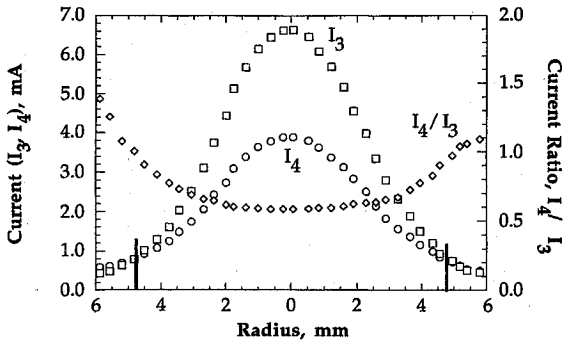

Fig. 10 Probe currents I_3, I_4, and I_4/I_3 giving $u_i/c_{m,H^+} \sim 1$ on the thruster centerline.

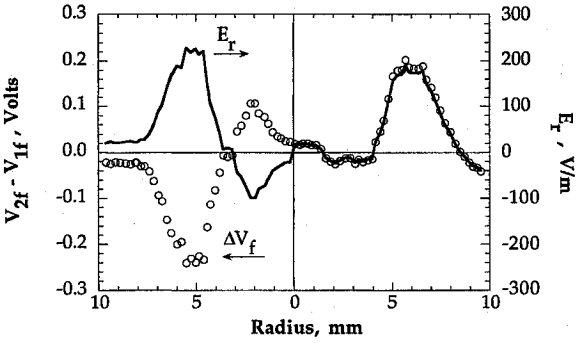

Fig. 11 $V_{2f} - V_{1f}$ measurement with radial double-probe configuration. Also shown is the resulting radial E-field E_r vs position across the thruster face.

3), so that the uncertainty in the ion speed ratio is influenced primarily by knowledge of the plasma state at the exit-plane.

Floating-Probe Measurements

A double floating-probe configuration (electrodes P_1 and P_2 of Fig. 2) was used to estimate E_r near the thruster exit-plane. For two floating probes in a plasma with electrode sheath potentials V_{s1} and V_{s2}, and a measured floating potential difference between the two electrodes $\Delta V_f = V_{f2} - V_{f1}$, the difference in the plasma potential ΔV_p between the two electrodes is related to ΔV_f by

$$\Delta V_p = \Delta V_f - (V_{s2} - V_{s1}) \tag{18}$$

The result of a typical ΔV_f measurement is plotted in Fig. 11. The sign reversal of the signal for the two peaks ($|\Delta V_f| \approx 0.2$ V) at $r = 5.5$ mm is a consequence of electrode orientation remaining constant during a probe sweep while the plasma potential gradient changes sign across the plume. From Eq. (18), ΔV_p can be found from ΔV_f and the probe sheath drops. For a single floating electrode, the sheath potential drop V_s is derived by summing the ion and electron current into the probe and solving for the potential that satisfies the zero net current requirement.[38] This yields an electrode sheath potential of

$$V_s = \frac{kT_e}{2e}\,\ell n\left(\frac{m_i}{m_e}\frac{T_e}{T_i}\right) \tag{19}$$

Since the logarithm term does not vary by more than 2% over the electrode separation, the difference in electrode sheath potentials is

$$V_{s2} - V_{s1} = \Delta V_s \cong [\Delta(kT_e)/2e]\ell n[(m_i/m_e)(T_e/T_i)] \tag{20}$$

Near the thruster centerline, the change in T_e over the 1.4-mm electrode separation [$\Delta(kT_e)$] is slight because of the measured flat T_e profile and the shape of the profile near the centerline. For a $\Delta(kT_e)$ as large as 0.01 eV (~500 K), ΔV_s is <0.04 V, allowing the sheath drop to be neglected in Eq. (18). Therefore, $\Delta V_f \approx V_{p2} - V_{p1}$, generated by E_r at the thruster exit-plane. The resulting plot of E_r vs radial position is also shown in Fig. 11. The field is approximately zero at the center as expected, and is radially inward inside the plume, with a peak of ~100 V/m near $r = 2$ mm. The field apparently peaks at ~200 V/m at $r \approx 5$ mm, but this is likely a consequence of large gradients in T_e and n_e at the plume edge, voiding the assumption of small ΔV_s. For $r < 4$ mm, $\Delta V_f < 0.1$ V, and this correction to V_{d2} [see Eqs. (17) and (18)] has been ignored.

The floating-probe measurements of E_r are evidence for the existence of current density and ohmic heating in the near-field plume. From the measured n_e, the estimated ionization fraction on the centerline is $\alpha \approx 10^{-4}$, giving a plasma electrical conductivity of $\sigma \approx 100$ Ω/m. In the exit-plane (at $r = 2$ mm) $E_r \sim 100$ V/m, which is equivalent to $j_r = \sigma E_r \sim 1$ A/cm^2. If this current is flowing across an area of approximately 0.2 cm^2, the total current crossing the exit-plane amounts to ~0.2 A, or 2% of the total current supplied to the arcjet. Furthermore, this current represents a small amount of ohmic heating ($j^2/\sigma \sim 1$ W/cm^3) in the exit-plane region.

The indication of current in the near-field plume is consistent with the boundary condition that j must be perpendicular to the anode wall at a 20-deg angle to the centerline, forcing a current component perpendicular to the exit-plane in the plume. These measurements carry implications for downstream boundary conditions for arcjet numerical models.

Summary and Conclusions

The use of millimeter-size, thin-sheath electrostatic probes in the exit-plane region of a low-power arcjet provides a low-cost and robust means for measuring plasma parameters. In small arcjet devices, it is necessary to account for the effect of radial and axial gradients on probe output, allowing single-, triple-, and quadruple-electrostatic probes to be employed for measurements of T_e, n_e, and $u_i/c_{m,H^+}$. A technique has been presented for analyzing probe data in the presence of these gradients, resulting in symmetric T_e and n_e radial profiles. Using a double floating-probe mode, E_r can also be measured accurately near the centerline in the near-field plume.

Single-probe radial surveys have displayed the symmetrical nature of the arcjet plume and independently serve to verify T_e measurements made with triple and quadruple probes. An improved quadruple-probe theory, showing excellent agreement with independent triple-probe surveys, provides radial and centerline axial profiles of T_e and n_e near the exit-plane. While the axial gradient in n_e is small over $2.2 < x < 6.2$ mm, comparison with interior nozzle n_e measurements indicates that the density varies by 1–2 orders of magnitude at the exit-plane. For $x = 2.2$ mm, quadruple-probe measurements yield $T_e = 6600$ K ± 15%, $n_e = 3.6 \times 10^{12}$ cm^{-3} ± 60%, and $u_i/c_{m,H^+} = 1.0$ ± 15%. Floating-electrode measurements indicate that approximately 2% of the thruster current extends downstream of the thruster exit-plane.

Acknowledgments

This work was funded by the U.S. Air Force Office of Scientific Research under Contracts F49620-92-J-0448/0280. Mitat Birkan was the Program Manager. We gratefully acknowledge the arcjet thruster and PPU loaned by the Onboard Propulsion Branch of the NASA Lewis Research Center. We also acknowledge the assistance of N. T. Tiliakos and Gary F. Willmes with the experiments. We acknowledge the helpful discussions and assistance from R. P. Lucht, S. G. Del Medico, and T. W. Megli, and particularly from H. Krier. We wish to thank M. J. Wilson for help with the figures and data reduction, and W. Johnson and D. W. Foley for machining.

References

[1]Rhodes, R., and Keefer, D., "Non-Equilibrium Modeling of Hydrogen Arcjet Thrusters," *Proceedings of the 23rd International Elec-*

tric Propulsion Conference (Seattle, WA), Electric Rocket Propulsion Society, Columbus, OH, 1993, pp. 2020–2031.

[2]Miller, S., and Martinez-Sanchez, M., "Nonequilibrium Numerical Simulation of Radiation-Cooled Arcjet Thrusters," *Proceedings of the 23rd International Electric Propulsion Conference* (Seattle, WA), Electric Rocket Propulsion Society, Columbus, OH, 1993, pp. 2032–2050.

[3]Butler, G. W., Kull, A. E., and King, D. Q., "Numerical Simulations of Hydrogen Arcjet Performance," *Proceedings of the 23rd International Electric Propulsion Conference* (Seattle, WA), Electric Rocket Propulsion Society, Columbus, OH, 1993, pp. 2252–2263.

[4]Ciucci, A., d'Agostino, L., and Andrenucci, M., "Development of a Numerical Model of the Nozzle Flow in Low Power Arcjet Thrusters," *Proceedings of the 23rd International Electric Propulsion Conference* (Seattle, WA), Electric Rocket Propulsion Society, Columbus, OH, 1993, pp. 1662–1674.

[5]Megli, T. W., Krier, H., Burton, R. L., and Mertogul, A. E., "Two Temperature Modeling of N_2/H_2 Arcjets," AIAA Paper 94-2413, June 1994.

[6]Megli, T. W., Krier, H., and Burton, R. L., "A Plasmadynamics Model for Nonequilibrium Processes in N_2/H_2 Arcjets," AIAA Paper 95-1961, June 1995.

[7]Carney, L. M., and Keith, T. G., "Langmuir Probe Measurements of an Arcjet Exhaust," *Journal of Propulsion and Power*, Vol. 5, No. 3, 1989, pp. 287–294.

[8]Carney, L. M., and Sankovic, J. M., "The Effects of Arcjet Operating Condition and Constrictor Geometry on the Plasma Plume," AIAA Paper 89-2723, July 1989.

[9]Sankovic, J. M., "Investigation of the Arcjet Plume Near Field Using Electrostatic Probes," NASA TM-103638, Nov. 1990.

[10]Sankovic, J., and Jankovsky, R., "An Experimental Investigation of the Effective Current Collecting Area of a Spherical Langmuir Probe in an Arcjet Thruster Exhaust," AIAA Paper 90-0073, Jan. 1990.

[11]Gallimore, A. D., Kim, S.-W., Foster, J. E., King, L. B., and Gulczinski, F. S., "Near and Far-Field Plume Studies of a 1-kW Arcjet," AIAA Paper 94-3137, June 1994.

[12]Mott-Smith, H. M., and Langmuir, I., "The Theory of Collectors in Gaseous Discharges," *Physical Review*, Vol. 28, Second Series, July–Dec. 1926, pp. 727–763.

[13]Chen, S.-L., and Sekiguchi, T., "Instantaneous Direct-Display System of Plasma Parameters by Means of Triple Probe," *Journal of Applied Physics*, Vol. 36, No. 8, 1965, pp. 2363–2375.

[14]Tilley, D. L., Kelly, A. J., and Jahn, R. G., "The Application of the Triple Probe Method to MPD Thruster Plumes," AIAA Paper 90-2667, July 1990.

[15]Gallimore, A. D., Kelly, A. J., and Jahn, R. G., "Anode Power Deposition in Quasisteady Magnetoplasmadynamic Thrusters," *Journal of Propulsion and Power*, Vol. 8, No. 6, 1992, pp. 1224–1231.

[16]Tilley, D. L., Gallimore, A. D., Kelley, A. J., and Jahn, R. G., "The Adverse Effect of Perpendicular Ion Drift Flow on Cylindrical Triple Probe Electron Temperature Measurements," *Review of Scientific Instruments*, Vol. 65, No. 3, 1994, pp. 678–681.

[17]Paccani, G., "Electrostatic Probe Diagnostics of Solid Propellant MPD Thruster Jets," AIAA Paper 94-3340, June 1994.

[18]Pobst, J. A., Schilling, J. H., Erwin, D. A., and Spores, R. A., "Time Resolved Measurements of 1-kW Arcjet Plumes Using Current Modulation Velocimetry and Triple Langmuir Probes," *Proceedings of the 23rd International Electric Propulsion Conference* (Seattle, WA), Electric Rocket Propulsion Society, Columbus, OH, 1993, pp. 1177–1184.

[19]Habiger, H. A., Auweter-Kurtz, M., and Kurtz, H., "Electrostatic Probes for the Investigation of Arc-Driven Electric Propulsion Devices," *Proceedings of the 23rd International Electric Propulsion Conference* (Seattle, WA), Electric Rocket Propulsion Society, Columbus, OH, 1993, pp. 1137–1147.

[20]Kanal, M., "Theory of Current Collection of Moving Cylindrical Probes," *Journal of Applied Physics*, Vol. 35, No. 6, 1964, pp. 1697–1703.

[21]Bruce, C., and Talbot, L., "Cylindrical Electrostatic Probes at Angles of Incidence," *AIAA Journal*, Vol. 13, No. 9, 1975, pp. 1236–1238.

[22]Johnson, B. H., and Murphree, D. L., "Plasma Velocity Determination by Electrostatic Probes," *AIAA Journal*, Vol. 7, No. 10, 1969, pp. 2028–2030.

[23]Poissant, G., and Dudeck, M., "Velocity Profiles in a Rarefied Argon Plasma Stream by Crossed Electrostatic Probes," *Journal of Applied Physics*, Vol. 58, No. 5, 1985, pp. 1772–1779.

[24]Burton, R. L., DelMedico, S. G., and Andrews, J. C., "Application of a Quadruple Probe Technique to MPD Thruster Plume Measurements," *Journal of Propulsion and Power*, Vol. 9, No. 5, 1993, pp. 771–777.

[25]DelMedico, S. G., "Plasma Flow Measurements by a Quadruple Probe in a Quasi-Steady MPD Plasma," M.S. Thesis, Univ. of Illinois, Urbana, IL, 1992.

[26]Bufton, S. A., "Electrostatic Probe Measurements of a Low-Power Hydrazine Arcjet Exhaust," Ph.D. Dissertation, Univ. of Illinois, Urbana, IL, 1995.

[27]Burton, R. L., Bufton, S. A., Tiliakos, N. T., and Krier, H., "Application of Multiple Electrostatic Probes to a Low Power Arcjet," AIAA Paper 94-3299, June 1994.

[28]Bufton, S. A., Burton, R. L., and Krier, H., "Measured Plasma Properties at the Exit Plane of a 1-kW Arcjet," AIAA Paper 95-3066, July 1995.

[29]*Omega CC High Temperature Cement and Binder*, Omega Engineering, Inc., Stamford, CT.

[30]Chung, P. M., Talbot, L., and Touryan, K. J., *Electric Probes in Stationary and Flowing Plasmas: Theory and Application*, Springer–Verlag, New York, 1975.

[31]Nachtrieb, R. T., "Application of the Saha Equation to High Temperature (>6000 K) Rocket Exhaust," Phillips Lab., PL-TR-92-3042, Edwards AFB, CA, Jan. 1993.

[32]Keefer, D., Moeller, T., and Rhodes, R., "Multiplexed Laser-Induced Fluorescence and Nonequilibrium Processes in Arcjets," AIAA Paper 94-2656, June 1994.

[33]Hargus, W., Micci, M., and Spores, R., "Interior Spectroscopic Investigation of the Propellant Energy Modes in an Arcjet Nozzle," AIAA Paper 94-3302, June 1994.

[34]Curran, F. M., and Haag, T. W., "Extended Life and Performance Test of a Low-Power Arcjet," *Journal of Spacecraft and Rockets*, Vol. 29, No. 4, 1992, pp. 444–452.

[35]Manzella, D. H., Curran, F. M., Myers, R. M., and Zube, D. M., "Preliminary Plume Characteristics of an Arcjet Thruster," AIAA Paper 90-2645, July 1990.

[36]Zube, D. M., and Myers, R. M., "Techniques for Spectroscopic Measurements in an Arcjet Nozzle," *Journal of Propulsion and Power*, Vol. 8, No. 1, 1992, pp. 254–256.

[37]Pobst, J. A., Wysong, I. J., and Spores, R. A., "Laser Induced Fluorescence of Ground State Hydrogen Atoms in an Arcjet Plume," International Electric Propulsion Conf., Paper 95-28, Sept. 1995.

[38]Schott, L., "Electrical Probes," *Plasma Diagnostics*, edited by W. Lochte-Holtgreven, Wiley, New York, 1968, pp. 671–673.